Journal of Natural Gas Science and Engineering 33 (2016) 483–496

Contents lists available at ScienceDirect

Journal of Natural Gas Science and Engineering

journal homepage: www.elsevier.com/locate/jngse

A multi-continuum multi-phase parallel simulator for large-scale conventional and unconventional reservoirs

Kun Wang*, Hui Liu, Jia Luo, Zhangxin Chen

University of Calgary, Canada

ARTICLE INFO

Article history:
Received 22 February 2016
Received in revised form
3 May 2016
Accepted 11 May 2016
Available online 18 May 2016

Keywords:
Parallel simulator
Black oil models and compositional model
Fractured reservoirs
Nonlinear and linear solvers
Adaptive linear solver
Large-scale reservoir simulation

ABSTRACT

Reservoir simulation is considered as the core of data analysis during the development of an oilfield. With higher requirements from reservoir engineers, high-resolution geological model problems are commonly used in reservoir simulation. To simulate this kind of large-scale reservoir problems, based on black-oil models and compositional model, a parallel simulator is developed in this paper. Cartesian and corner point grids are supported by our simulator to describe complex geology, including faults and pinch-outs. The multi-continuum models (including a dual-porosity model, a dual-porosity dual-permeability model, and a multiple interacting continua model) are used to simulate fractured reservoirs. Geomechanics effects are successfully involved through a flexible and convenient interface provided by our simulator. Krylov subspace linear solvers, restricted additive Schwarz method, incomplete LU factorization (ILU) preconditioner, and a family of CPR (constrained pressure residual)-type preconditioners are implemented to provide flexibility of the linear system solution processes. Moreover, a new adaptive preconditioning strategy, which can automatically select and change preconditioner between a CPR-type preconditioner and an ILU preconditioner, is designed to accelerate the solution processes and is considered as the most efficient preconditioning technique to our knowledge. MPI-based parallel implementation is employed for each module of the simulator. With the simulator we developed, various conventional and unconventional reservoir simulation problems with large-scale geological models can be achieved on parallel computers within practical computational time. The computational efficiency and parallel scalability are achieved by our high-quality parallel implementation and efficient nonlinear and linear solution techniques.

© 2016 Elsevier B.V. All rights reserved.

1. Introduction

Reservoir simulation has become an important part of the oil and gas production business over the last 50 years. Reservoir simulation provides the reservoir engineers a reliable and efficient way to estimate reserves, and to diagnose and improve the oil recovery processes, which is enabled by advances in computing hardware, software design, and improved mathematical models and numerical algorithms.

For the mathematical models, the black oil model (Chen et al., 2006) is the most mature one and has been widely used by oil companies. However, for the unconventional oil and gas reservoirs, more complex mathematical models are necessary to describe the fluid properties. Some extended black oil models (Chen et al., 2006), which can handle gas condensate, volatile oil and multi-components, are developed to model a reservoir more accurately. The EOS-based compositional model is a more complex model that brings much more computation of phase flash calculation, while it gives the most accurate prediction of phase behavior. For natural fractures and hydraulic fractures, which are commonly seen in tight and shale oil and gas reservoirs, the dual-porosity/dual-permeability model and the multiple interacting continua (MINC) model (Pruess et al, 1985; Wu et al, 1988) homogenize the fractures and use superpositioned cells to represent the fractures and the matrix. The multiple-continuum approaches have been successfully applied to a wide range of unconventional reservoir problems. In (Wu et al., 2006, 2011), the fractured vuggy rocks are considered as a triple- or multiple-continuum medium, consisting of highly permeable and well-connected fractures, low-permeability rock matrix, and various-sized vugs. In (Wu et al., 2013), a hybrid multiple-continuum-medium modeling approach is developed to describe different types of fractures, including hydraulic fractures,

* Corresponding author.
E-mail address: wang30@ucalgary.ca (K. Wang).

http://dx.doi.org/10.1016/j.jngse.2016.05.040
1875-5100/© 2016 Elsevier B.V. All rights reserved.

natural fracture network, and micro fractures. In (Moinfar et al., 2013; Jiang et al., 2014), explicit fracture models are coupled with MINC model for the simulation of unconventional reservoirs. A unified framework model is developed in (Wu et al., 2014), which is able to incorporate known mechanisms and processes (gas adsorption and desorption, geomechanics effect, Klinkenberg or gas-slippage effect and non-Darcy flow) and use a hybrid fracture-modeling approach to simulate the unconventional gas reservoirs. In (Jiang et al.), two alternative hybrid approaches that aim at combining the advantages of multi-continuum and discrete-fracture/matrix representations are developed to adequately capture the effects of the multiscaled fracture system. For fractured reservoirs, another important factor that should be taken into consideration is geomechanics effect. A coupled geomechanics and reservoir flow model is a more accurate tool to model rock properties that are sensitive to stress changes, and to perform reliable history matching and recovery predictions. Also, it can be used to monitor the stress state during a recovery process in order to avoid economic losses and environmental issues that come along with the phenomena such as reservoir subsidence, rock mechanical failure, and wellbore damages due to subsurface fluid loss. A variety of methods, mainly three types of methods (explicit coupling, iterative coupling, and fully coupling), for coupling fluid flow and geomechanics have been proposed (Dean et al., 2006; Gutierrez et al., 2001; Minkoff et al., 2003; Tran et al., 2009) and have been successfully applied for unconventional reservoir simulations (Wang et al, 2014b; Winterfeld and Wu, 2014; Xiong et al., 2013, 2015).

For linear solvers, the ILU (incomplete LU factorization) preconditioned (Wallis et al, 1983; Behie and Forsyth, 1984) Krylov subspace methods (Saad, 1981) are usually employed as the default solvers by most of the commercial software. However, the ILU preconditioners are not effective enough for large-scale problems with highly heterogeneous permeability, which may lead to hundreds of linear iterations or even failure of a linear solver. To improve the effectiveness of a preconditioner, the CPR (constrained pressure residual) (Wallis et al., 1985; Cao et al., 2005) preconditioner employs two stages of preconditioning processes to handle the pressure systems and the global systems sequentially. At the first stage of the CPR preconditioner, due to the elliptic property of the pressure systems, algebraic multigrid methods are usually used to solve the pressure systems (Stüben, 2001; Stueben et al., 2007). The ILU preconditioners are used as global smoothers in the second stage of the CPR preconditioner. Based on the similar ideas, a family of CPR-type preconditioners, such as the FASP (fast auxiliary space preconditioning) preconditioner (Hu et al., 2011) and the CPR-FPF (F is to represent the preconditioning process for the full system, and P is to represent the preconditioning process for the pressure system) preconditioner (Wang et al., 2015; Liu et al., 2016), are developed.

With the advanced development of the petroleum industry, high resolution geological model is more frequently used by reservoir simulations to capture fine phenomena and get more accurate prediction of oil production (Cominelli et al., 2014). The corresponding reservoir models often contain more than millions of gird cells. There are two main issues of common commercial simulators for these large-scale reservoir simulation problems. Firstly, most of the commercial simulators are designed for personal computers or workstations, but the memory of these machines may not satisfy the requirement of large-scale problems, such as a full-field reservoir model with billions of gird cells. Secondly, the long simulation time, usually hours or even days, significantly reduces the work efficiency. To conquer these two issues, parallel computation techniques have been involved in reservoir simulations. Since 1980s, various of parallel simulators were developed (Li et al., 1995; Wheeler and Smith, 1989; Rutledge et al., 1991; Shiralkar et al., 1997; Parashar et al., 1997; Kaarstad et al., 1995; Killough and Bhogeswara, 1991; Killough et al., 1997). In (Dogru et al., 2002, 2009), Dogru et al. developed a parallel simulator, GigaPOWERS, which has been successfully applied to a case with one billion gird cells, and a truncated Neumann series preconditioner is developed. In (DeBaun et al., 2005), an object-oriented, component-based architecture is designed, built on which a black oil simulator and a compositional simulator are developed.

In this paper, we present a parallel simulator, which is designed for both personal computers and clusters. The objective of this simulator to provide the reservoir engineer with a strong and efficient tool for industrial use. The simulator employs parallel computation for every part of the simulation, including the grid generation and partition, data and well management, compressed sparse row storage for matrices, preconditioners and linear solvers, and implementation of physical models. Compared with the parallel simulators developed in the above literature, our simulator has the following features: (1) for the girds, it supports corner point grids, which enable it to handle faults and complex geology; (2) for the mathematical models, it implements various black-oil based models and compositional model, which is suitable for practical simulation of conventional and unconventional reservoirs; (3) for fractured reservoirs, it employs the multiple-continuum approaches to simulate the fractured reservoirs, and uses a flexible and convenient interface to couple other geomechanics software packages and get geomechanics effects involved in simulations; (4) for linear solvers, it employs the CPR-type preconditioners and a new adaptive preconditioning strategy in the linear system solution processes, which is considered as the most efficient method to our knowledge; (5) for parallel computing, it employs MPI-based parallel implementation for each module of the simulator and employs advanced parallel algorithms, such as the Hilbert Space-filling Curve method, parallel multigrid algebraic method and restricted additive Schwarz method, to ensure the computational efficiency and parallel scalability. The rest of this paper is organized as follows: In Section 2–6, we demonstrate the design of our simulator with details on the supported grid types and mathematical models, fracture modeling, nonlinear and linear solution methods, and their parallel implementation; in Section 7, we validate our simulator with commercial simulators by comparing benchmarks and show various functions and features of our simulator for solving practical problems, as well as the parallel efficiency of the solution methods and total simulation time; in Section 8, we draw the conclusions.

2. Grids and numerical flux

Regular Cartesian grid is the most frequently used grid in reservoir simulations. Cells in such a grid are unit cubes and may be simply identified by their index values (i,j,k); see the left figure in Fig. 1. For the Cartesian grid, the calculation of the flux across a face is simple, which only employs the properties on the local cell and its direct neighbouring cell. It is called two-point flux-approximation (TPFA) scheme. The TPFA scheme results in a 5-point scheme in 2D and a 7-point scheme in 3D, which makes the linearized Jacobian systems easy to solve. However, it is difficult for the regular Cartesian grids to describe a complex geological model, such as the reservoirs with pinch-outs and faults. To describe such model precisely, it is necessary to define the position of a grid cell by its corner point locations. Then the grid consists of hexahedra and each hexahedron is shaped with eight corners and bilinear planes as surfaces. This kind of grid is called corner point grid; see the middle and right figures in Fig. 1. When a corner point grid and/or a permeability tensor are used, the TPFA scheme can lead to an

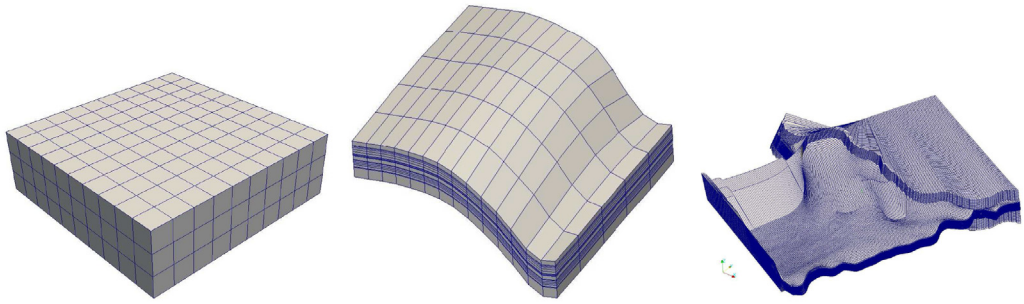

(a) Cartesian grid (b) corner point grid (c) corner point grid

Fig. 1. Grids.

inconsistent finite difference method and significant errors if the grid is highly distorted. Hence, the multi-point flux-approximation (MPFA) scheme should be used, which may result in a 9-point scheme in 2D and 27-point scheme in 3D. In our simulator, both regular Cartesian grids and corner point grids are supported, and the TPFA scheme or the MPFA scheme is automatically chosen according to the used grids.

3. Mathematical model

Two types of mathematical models are supported in our simulator. The first type of models are based on the standard black oil model. The second type of model is the EOS-based compositional model.

The black oil model assumes that: 1) three phases (oil, water and gas) coexist in the reservoir; 2) oil can only exist in the oil phase; 2) water can only exist in the water phase; 3) gas can exist both in the oil and gas phase; 4) the reservoir is isothermal. Combining Darcy's law and mass conservation law for each component, the black oil model can be written as:

$$\begin{cases} \dfrac{\partial}{\partial t}\left(\dfrac{\phi s_o}{b_o}\right) = \nabla\cdot\left(\dfrac{\mathbf{K}K_{ro}}{\mu_o b_o}\nabla\Phi_o\right) + q_o, \\ \dfrac{\partial}{\partial t}\left(\dfrac{\phi s_w}{b_w}\right) = \nabla\cdot\left(\dfrac{\mathbf{K}K_{rw}}{\mu_w b_w}\nabla\Phi_w\right) + q_w, \\ \dfrac{\partial}{\partial t}\left(\dfrac{\phi r_s s_o}{b_o}\right) + \dfrac{\partial}{\partial t}\left(\dfrac{\phi s_g}{b_g}\right) = \nabla\cdot\left(\dfrac{\mathbf{K}K_{ro}r_s}{\mu_o b_o}\nabla\Phi_o\right) + \nabla\cdot\left(\dfrac{\mathbf{K}K_{rg}}{\mu_g b_g}\nabla\Phi_g\right) + q_o + q_g, \end{cases} \tag{1}$$

where ϕ and $\mathbf{K}$ are porosity and permeability, r_s is the solution gas-oil ratio for saturated oil, for phase α ($\alpha = o,w,g$), Φ_α is potential, and s_α, μ_α, p_α, b_α, $K_{r\alpha}$ and q_α are the saturation, viscosity, pressure, formation volume factor, relative permeability and production rate, respectively. These variables have the following relations:

$$\Phi_\alpha = p_\alpha + \rho_\alpha^m \wp z,$$

$$s_o + s_w + s_g = 1,$$

$$p_w = p_o - p_{cow}(s_w),$$

$$p_g = p_o + p_{cog}(s_g),$$

where ρ_α^m is the mass density of phase α, $p_{co\alpha}$ are the capillary pressure between oil phase and α phase, $\wp$ is the gravitational constant and z is the reservoir depth.

In order to use the black oil model to simulate the gas condensate and the volatile oil reservoirs, the second assumption of the black oil model should be modified as: oil can exist both in the oil and gas phase. The oil content for condensate saturated gas, r_v, is included to describe the oil-gas ratio for the saturated gas. Then the oil component conservation equation in Eqn. (1) is modified as

$$\frac{\partial}{\partial t}\left(\frac{\phi s_o}{b_o}\right) + \frac{\partial}{\partial t}\left(\frac{\phi s_g r_v}{b_g}\right) = \nabla\cdot\left(\frac{\mathbf{K}K_{ro}}{\mu_o b_o}\nabla\Phi_o\right) + \nabla\cdot\left(\frac{\mathbf{K}K_{rg}r_v}{\mu_g b_g}\nabla\Phi_g\right) + q_o + q_g. \tag{2}$$

To study a reservoir with oil gravity variation, an option called API tracking (Beraldo et al., 2007) is usually involved in the black oil model. With the API tracking option, two oil components are allowed in the oil phase, which are called "heavy" component and "light" component. The properties of "heavy" and "light" components, such as r_s and b, are different and are determined by their own PVT tables. Then the oil component conservation equation is separated into two equations for "heavy" component and "light"

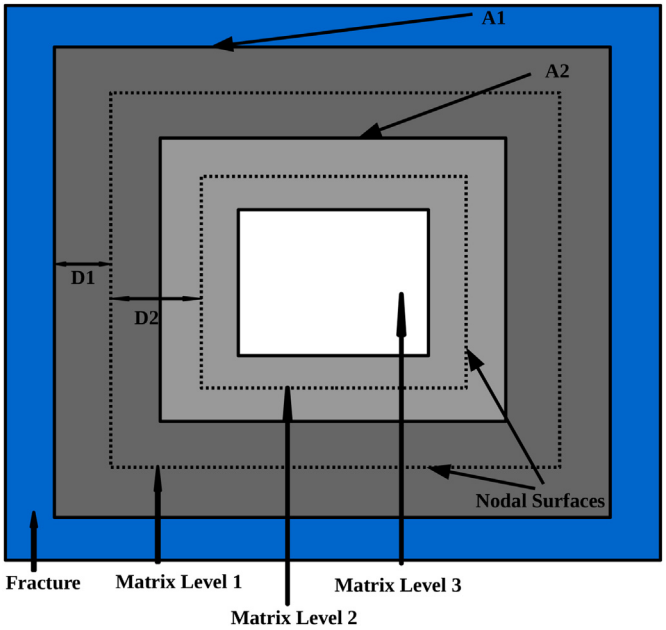

Fig. 2. MINC model: the cell is divided into a fracture sub-cell and three matrix sub-cells.

Algorithm 1
Adaptive Linear Solver: ALS($\varepsilon, \mathscr{N}_e, \varepsilon_a^0, \varepsilon_s$).

1: Calculate the expected convergence rate R_e:

$$R_e = e^{\frac{1}{\mathscr{N}_e}}. \tag{23}$$

2: Calculate the initial absolute residual ε_a.
3: If

$$\frac{\varepsilon_a}{\varepsilon_a^0} > \varepsilon_s, \tag{24}$$

then goto 4; else goto 6.
4: Setup RAS-ILU preconditioner.
5: Employ RAS-ILU preconditioned GMRES method to solve the linear system.
If the relative residual $e < \varepsilon$, stop; else, calculate the convergence rate R_{ILU}:

$$R_{\mathrm{ILU}} = e^{\frac{1}{\mathscr{N}_{\mathrm{ILU}}}}, \tag{25}$$

where $\mathscr{N}_{\mathrm{ILU}}$ is the number of RAS-ILU preconditioned GMRES iterations. If $R_{\mathrm{ILU}} < R_e$, continue the RAS-ILU preconditioned GMRES iteration; else, goto 6.
6: Setup the CPR-FPF preconditioner.
7: Employ the CPR-FPF preconditioned GMRES method with the solution from RAS-ILU preconditioned iterations as the initial guess. If the relative residual $e < \varepsilon$, stop; else, continue the CPR preconditioned GMRES iteration.

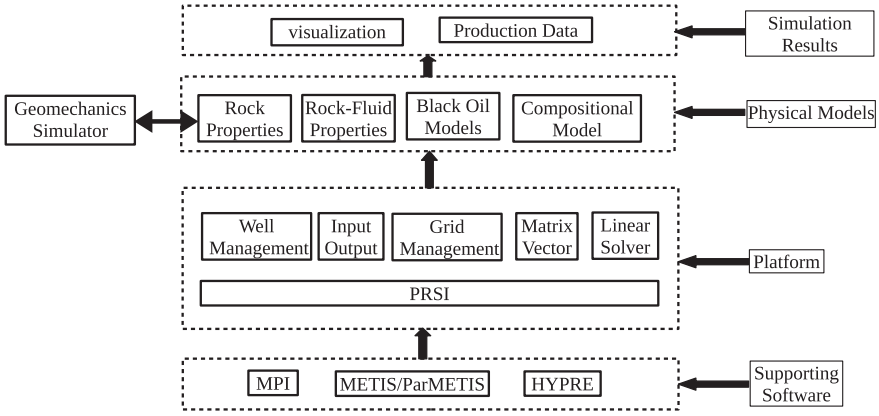

Fig. 3. Structure of the simulator.

component:

$$\begin{cases} \dfrac{\partial}{\partial t}\left(\dfrac{\phi s_o C_h}{b_{o,h}}\right) = \nabla\cdot\left(\dfrac{\mathbf{K}K_{ro}C_h}{\mu_o b_{o,h}}\nabla\Phi_o\right) + q_{o,h}, \\ \dfrac{\partial}{\partial t}\left(\dfrac{\phi s_o C_l}{b_{o,l}}\right) = \nabla\cdot\left(\dfrac{\mathbf{K}K_{ro}C_l}{\mu_o b_{o,l}}\nabla\Phi_o\right) + q_{o,l}, \end{cases} \tag{3}$$

where $()_h$ $()_l$ and are the variables for "heavy" and "light" component respectively, C is the concentration, and $\mu_o = C_h\mu_h + C_l\mu_l$. The gas component conservation equation also needs to be modified as

$$\begin{aligned} &\frac{\partial}{\partial t}\left(\phi s_o\left(\frac{r_{s,h}}{b_{o,h}} + \frac{r_{s,l}}{b_{o,l}}\right)\right) + \frac{\partial}{\partial t}\left(\frac{\phi s_g}{b_g}\right) \\ &= \nabla\cdot\left(\frac{\mathbf{K}K_{ro}}{\mu_o}\left(\frac{r_{s,h}}{b_{o,h}} + \frac{r_{s,l}}{b_{o,l}}\right)\nabla\Phi_o\right) + \nabla\cdot\left(\frac{\mathbf{K}K_{rg}}{\mu_g b_g}\nabla\Phi_g\right) + q_o + q_g, \end{aligned} \tag{4}$$

where

$$q_o = C_h q_{o,h} + C_l q_{o,l} \tag{5}$$

$$r_s = C_h r_{s,h} + C_l r_{s,l} \tag{6}$$

When polymer flooding is applied to improve the oil recovery rate, the mobility of the water decreases due to the polymer retention. Modification is required to the water equation and an additional equation for polymer mass conservation should be added to the black oil systems. The water and polymer equations can be written as follows

$$\frac{\partial}{\partial t}\left(\frac{\phi s_w}{b_w}\right) = \nabla\cdot\left(\frac{\mathbf{K}K_{rw}}{\mu_{w,\mathrm{eff}} b_w R_k}\nabla\Phi_w\right) + q_w, \tag{7}$$

$$\frac{\partial}{\partial t}\left(\frac{\phi s_w C_p}{b_w} + \rho_{r,\mathrm{ref}}\left(1-\phi_{\mathrm{ref}}\right)C_p^a\right) = \nabla\cdot\left(\frac{\mathbf{K}K_{rw}}{\mu_{p,\mathrm{eff}} b_w R_k}\nabla\Phi_o\right) + C_p q_w, \tag{8}$$

where C_p is the polymer concentration, ϕ_{ref} is the porosity at reference pressure, $\rho_{r,\mathrm{ref}}$ is the rock density at reference pressure, C_p^a is the polymer adsorption concentration, $\mu_{\alpha,\mathrm{eff}}$ is the effective viscosity of polymer ($\alpha = p$) and water ($\alpha = w$), and R_k is the relative permeability reduction factor for the aqueous phase due to polymer retention.

In the black-oil-based models, phase behavior is simply represented by b_o, b_g, r_s and r_v, which are only related with pressure, and flash calculations are not needed. Whenever it is inappropriate to use the black-oil-based models to describe the phase behavior, an EOS-based compositional model is required. In our simulator, three types of EOS are supported for the phase flash calculation, which

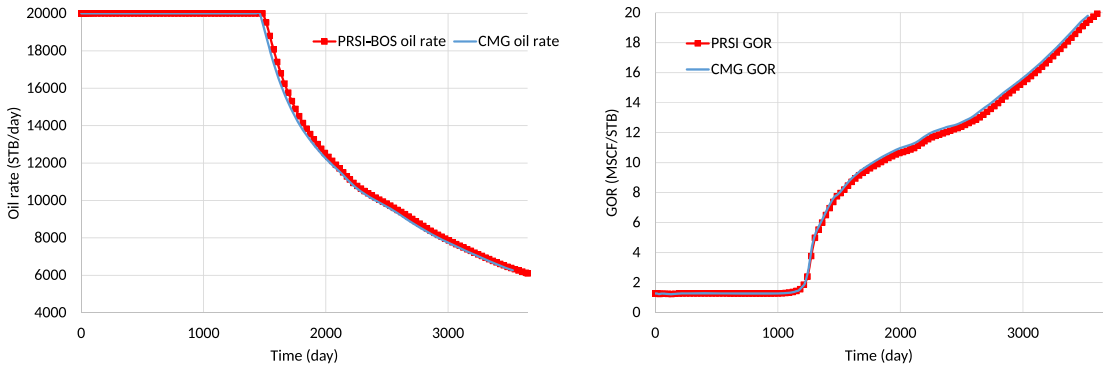

(a) oil rate

(b) GOR

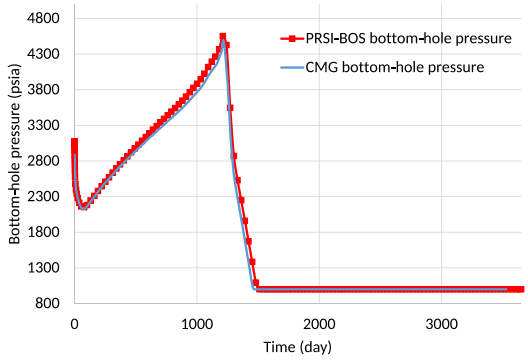

(c) bottom-hole pressure

Fig. 4. SPE1 case

are the Redlich-Kwong (Redlich and Kwong, 1949), Soave-Redlich-Kwong (Soave, 1972) and Peng-Robinson equation of state (Peng and Robinson, 1976). The mass conservation equations in compositional model can be represented as: for each hydrocarbon component (or pseudo-component) c,$c = 1,\cdots,n$ and for water

$$\frac{\partial}{\partial t}\left(\phi\left(s_o\rho_o x_c + s_g\rho_g y_c\right)\right) = \nabla\cdot\left(\frac{\mathbf{K}K_{ro}}{\mu_o}\rho_o x_c\nabla\Phi_o\right) + \nabla\cdot\left(\frac{\mathbf{K}K_{rg}}{\mu_g}\rho_g y_c\nabla\Phi_g\right) + \rho_o x_c q_o + \rho_g y_c q_g, \tag{9}$$

$$\frac{\partial}{\partial t}(\phi s_w\rho_w) = \nabla\cdot\left(\frac{\mathbf{K}K_{rw}}{\mu_w}\rho_w\nabla\Phi_w\right) + \rho_w q_w, \tag{10}$$

where x_c and y_c are the hydrocarbon component mole fractions in the oil phase and gas phase respectively, ρ_α are the mole density of phase α. In addition to the conservation equations, phase equilibrium equations for each hydrocarbon component are required. Since the water and the hydrocarbon components are totally separated in our model, only two-phase equilibrium relations between the oil phase and the gas phase are added to the whole system:

$$f_{c,o} = f_{c,g} \quad c = 1,\cdots,n, \tag{11}$$

where $f_{c,o}$ and $f_{c,g}$ are the fugacities of component c in oil and gas phases, respectively. The Tangent Plane Method (Michelsen, 1982) is employed for the phase stability analysis, and the combined ACSS (Accelerated Successive Substitution Method) (ACSS) (Mehra et al., 1983) and MVNR (Minimum Variable Newton-Raphson Method) (Fussell Yanosiket al, 1978) method is used for the phase split calculation.

For all the models supported by our simulator, fully implicit finite difference (volume) method is used to discretize and solve the nonlinear systems. The well constraints are modeled by the Peaceman model (Peaceman et al, 1983), and they are also solved implicitly.

4. Fracture models and geomechanics

To handle the natural and hydraulic fracture, a dual-porosity model and a dual-permeability model are implemented. For the dual-porosity model, a multiple interacting continua (MINC) approach is supported and the standard dual-porosity model is treated as a particular situation of the MINC model. For the MINC model, each cell can be divided into arbitrary number of sub-cells according to the user input; see Fig. 2. The MINC model (Pruess et al, 1985; Wu et al, 1988) involves discretization of matrix blocks into a sequence of nested volume elements, Fig. 2, which are defined on the basis of distances between nodal surfaces and the area of matrix surface, such as D_1, D_2 and A_1, A_2 in Fig. 2. Through this method, it is possible to resolve in detail the gradients (of pressure, temperature, etc.) that drive inter-porosity flow, and give more accurate prediction of multi-phase flow in fractured reservoirs than the dual-porosity model. In the MINC model, each matrix sub-cell can only connect with its nearest outer and inner sub-cells, and they cannot connect with matrix sub-cells in other cells. Taking the oil component conservation equation in the black oil model as

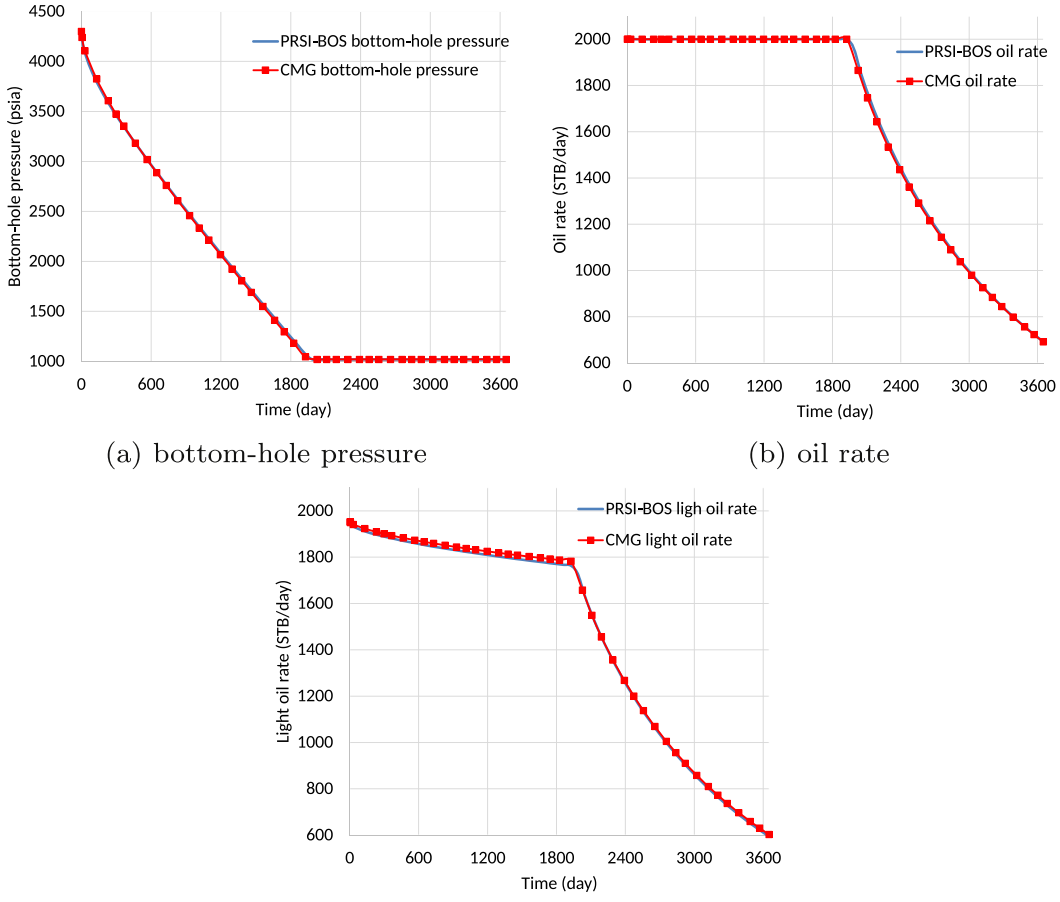

(a) bottom-hole pressure

(b) oil rate

(c) light oil rate

Fig. 5. API tracking case.

an example, we can represent the MINC model as follows:

$$\frac{\partial}{\partial t}\left(\frac{\phi_f s_{o,f}}{b_{o,f}}\right) = \nabla\cdot\left(\frac{\mathbf{K}_f K_{ro,f}}{\mu_{o,f} b_{o,f}}\nabla\Phi_{o,f}\right) - q_{o,fm} + q_{o,f}, \tag{12}$$

$$\frac{\partial}{\partial t}\left(\frac{\phi_{m_1} s_{o,m_1}}{b_{o,m_1}}\right) = q_{o,mf} - q_{o,m_1 m_2}, \tag{13}$$

$$\frac{\partial}{\partial t}\left(\frac{\phi_{m_k} s_{o,m_k}}{b_{o,m_k}}\right) = q_{o,m_k} - q_{o,m_k m_{k+1}}, \quad k = 2,\cdots,M-1, \tag{14}$$

$$\frac{\partial}{\partial t}\left(\frac{\phi_{m_M} s_{o,m_M}}{b_{o,m_M}}\right) = q_{o,m_{M-1} m_M}, \tag{15}$$

where $(\cdot)_f$ and $(\cdot)_{m_k}(k = 1,\cdots,M)$ are the variables for the fracture and the k-th matrix level respectively, $q_{o,fm}$ is the matrix-fracture transfer term, M is the number of matrix levels, $q_{o,m_k m_{k+1}}$ is the matrix-matrix transfer term between the k-th matrix level and the $(k+1)$-th matrix level. The transfer terms can be calculated by

$$q_{o,x_1x_2} = \omega\left(\frac{K_{ro}}{\mu_o b_o}\right)_t (p_{x_2} - p_{x_1}), \quad x_1 = m, m_1,\cdots,m_{M-1}, \quad x_2 = f, m_2,\cdots,m_M, \tag{16}$$

where, $(\cdot)_t$ is equal to x_1 or x_2 depending on which one is upstream, and ω is the shape factor. Gilman and Kazemi's (Gilman Kazemiet al, 1983) and Warren and Root's (Warren et al, 1963) shape factors are supported by our simulator. In order to consider the flow between matrix sub-cells in different cells, dual-permeability model should

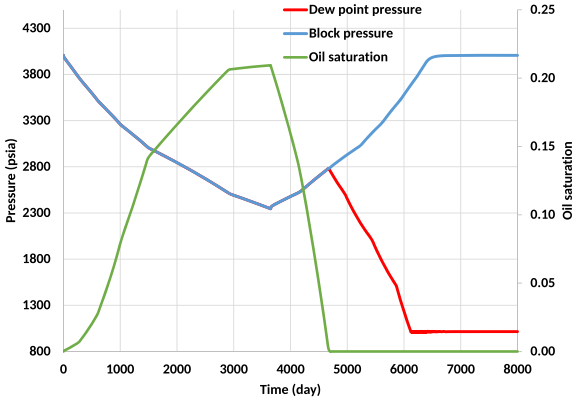

Fig. 6. Gas condensate case: pressure, dew point pressure and oil phase pressure at the well block

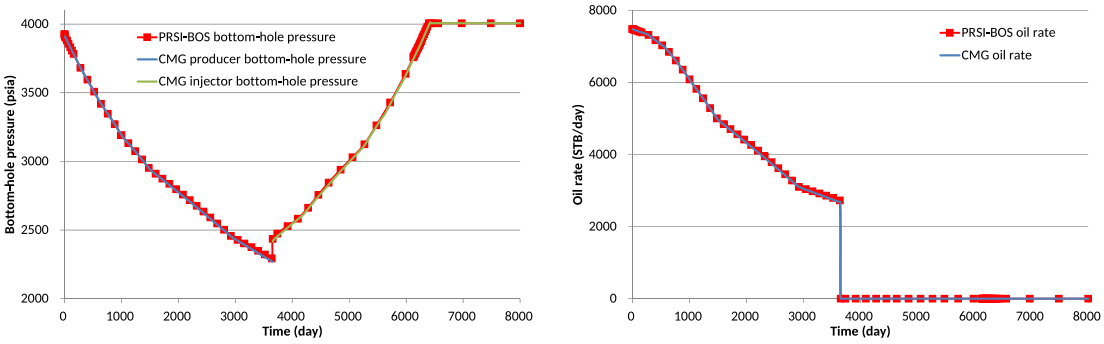

(a) bottom-hole pressure (b) oil rate

Fig. 7. Gas condensate case.

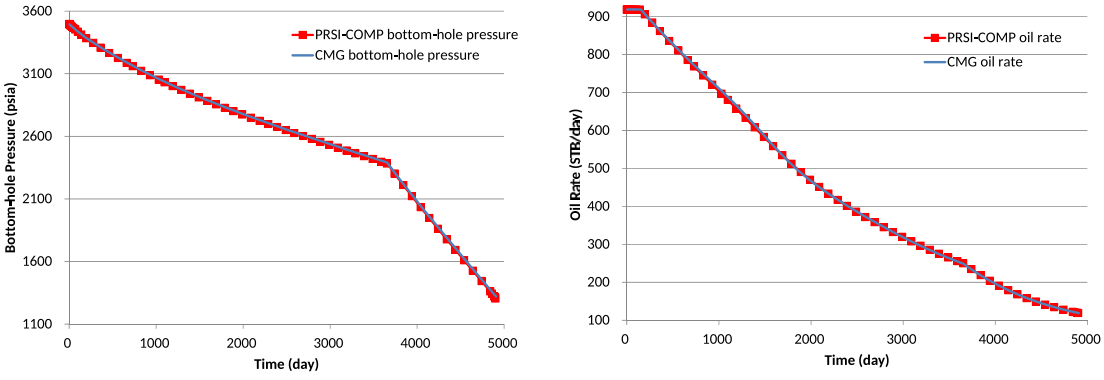

(a) bottom-hole pressure (b) oil rate

Fig. 8. SPE3 case.

be used. The mathematical description of dual-permeability model can be written as follows:

$$\frac{\partial}{\partial t}\left(\frac{\phi_f s_{o,f}}{b_{o,f}}\right) = \nabla\cdot\left(\frac{\mathbf{K}_f K_{ro,f}}{\mu_{o,f} b_{o,f}}\nabla\Phi_{o,f}\right) - q_{o,mf} + q_{o,f}, \tag{17}$$

$$\frac{\partial}{\partial t}\left(\frac{\phi_m s_{o,m}}{b_{o,m}}\right) = \nabla\cdot\left(\frac{\mathbf{K}_m K_{ro,m}}{\mu_{o,m} b_{o,m}}\nabla\Phi_{o,m}\right) + q_{o,mf}. \tag{18}$$

The dual-porosity/dual-permeability models for other extended black oil model and compositional model have the similar forms as the black oil model.

For conventional reservoirs, the effects of stress variation are usually ignored. Sequentially, the porosity is only related to the flow pressure, and the permeability keeps static during the simulation. However, for the unconventional reservoirs with natural or hydraulic fractures, the rock properties are sensitive to the stress changes. In order to perform more reliable simulation results, geomechanics effects should be included in our simulator. Usually, the stress can be calculated by finite element methods. Then with the stress, we can get the porosity and the permeability that are related to stress. An interface to geomechanics software packages is provided by our simulator. Through this interface, the value of porosity and permeability as well as their derivatives with respect to the pressure at each Newton iteration can be conveniently used as input by our simulator. Consequently, an iteratively coupled geomechanics and fluid flow reservoir simulator is achieved. In (Luo et al., 2015, 2016), our simulator has been successfully coupled with a geomechanics software package, and the simulation results have been validated by comparing benchmarks. Encouraging parallel speedup of coupled simulations for large-scale problems is also obtained in these papers.

5. Nonlinear and linear solvers

5.1. Nonlinear methods

The black oil based models and the compositional model are highly nonlinear systems. The Newton (also called Newton-Raphson) method is the most commonly used method for nonlinear problems. At each Newton iteration, the nonlinear system is linearized and a linear system is required to be solved accurately. For large-scale reservoir simulations, the computational cost of the accurate solution of the linear system is very expensive, and the convergence of the nonlinear iterations may not benefit from the accuracy of the solution very much. Hence, an inexact Newton method (Chen et al., ; Wang et al., 2015), which is described in Algorithm ??, is employed by our simulator. The main difference between the inexact Newton method and the standard Newton method is that the required residual is dynamically selected in the inexact Newton method. The convergence of the nonlinear iterations can be guaranteed by the inexact Newton method, just like the standard Newton method does. The main advantage of the inexact Newton method is to prevent the linear system from being oversolved. The required residual in the inexact Newton method

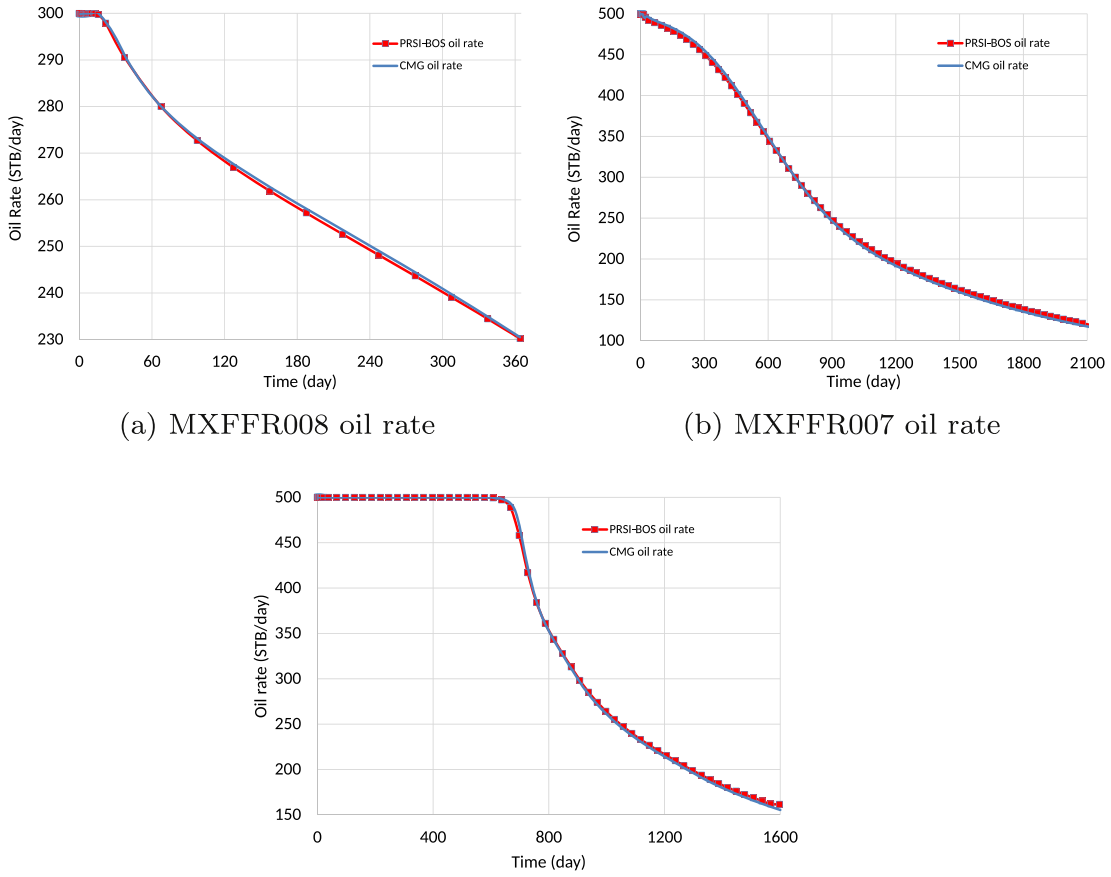

(a) MXFFR008 oil rate

(b) MXFFR007 oil rate

(c) MXFFR003 oil rate

Fig. 9. Dual-porosity/dual-permeability/MINC cases

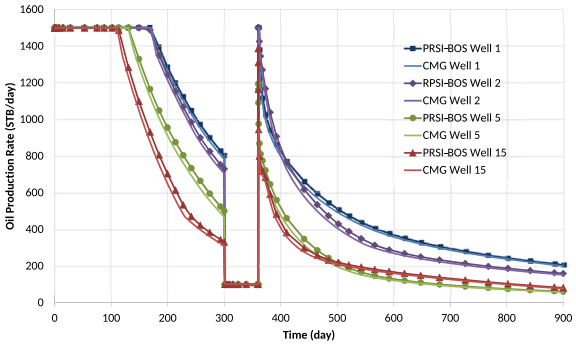

Fig. 10. SPE9: comparison with IMEX. Oil production rate of producer 1, 2, 5 and 15.

may be around 10^{-1} or 10^{-2} at the first several iterations, benefiting from which the computational time will be saved. More details about the inexact Newton method can be found in (Wang et al., 2015; Chen et al.,). The initial guess at the current time step is

Table 1
Refined SPE9 case: CPR-FPF solver and parallel scalability tests.

NP	Steps	Newton	Linear	Avg. L.	Time	Scal.
16	195	1121	3754	3.3	4825s	–
32	194	1079	3779	3.5	2971s	0.812
64	180	731	3187	4.4	1347s	0.896
128	180	747	3451	4.6	881s	0.685

Table 2
Refined SPE9 case: adaptive solver and parallel scalability tests.

NP	Steps	Newton	Linear	ILU/CPR	Avg. L.	Time	Scal.
16	185	1000	6275	4170/2105	6.3	4374s	–
32	187	1033	6664	4427/2237	6.5	2625s	0.833
64	183	923	6576	4308/2268	7.1	1248s	0.876
128	186	1060	7656	5099/2557	7.2	714s	0.766

Table 3
SPE10 black oil case: solver and parallel scalability tests.

NP	Steps	Newton	Linear	Avg. L.	Time	Scal.
16	419	1621	61,962	38.2	33,552s	–
32	419	1613	59,845	37.1	19,224s	0.873
64	419	1612	65,610	40.7	11,605s	0.723
128	419	1621	63,703	39.3	5758s	0.728

Table 4
SPE10-R2 black oil case: solver and parallel scalability tests.

NP	Steps	Newton	Linear	Avg. L.	Time	Scal.
256	300	1249	36,771	29.4	19,067s	–
512	300	1240	37,397	30.2	11,707s	0.814
768	300	1249	38,055	30.5	9508s	0.668
1024	300	1244	40,959	32.9	6423s	0.742

Table 5
SPE10-R2 black oil case: adaptive strategy tests.

NP	Steps	Newton	Linear	ILU/CPR	Avg. L.	Time
256	300	1241	37,872	18,144/19,728	30.5	14,272s
512	300	1253	39,194	18,762/20,432	31.3	9825s
768	300	1249	39,269	18,962/20,307	31.4	7341s
1024	300	1240	39,738	19,009/20,729	32.0	5475s

Table 6
MX521X469 case: solver and parallel scalability tests.

NP	Steps	Newton	Linear	Avg. L.	Time	Scal.
64	1525	5308	19,582	3.7	61,748s	–
128	1523	5286	19,869	3.8	33,721s	0.92
256	1531	5481	20,349	3.7	18,660s	0.83
512	1531	5423	20,748	3.8	9577s	0.81
1024	1536	5650	21,663	3.8	5474s	0.71

Table 7
MX521X469 case: adaptvie strategy tests.

NP	Steps	Newton	Linear	ILU/CPR-FPF	Avg. L.	Time	Scal.
64	1538	5737	51,626	44,693/6933	9.0	50,651s	–
128	1539	5826	54,220	46,821/7399	9.3	28,111s	0.90
256	1538	5768	55,398	48,025/7373	9.6	15,507s	0.82
512	1536	5733	57,588	49,774/7814	10.0	8524s	0.74
1024	1543	5970	61,900	54,264/7636	10.4	4873s	0.65

generally calculated through the linear extrapolation of the values of the last two time step. The extrapolation can improve the convergence the nonlinear iterations (Wang et al., 2015). However, the value of initial guess is chosen to be the same as the value of the last time step in case of a time-dependent boundary condition at the wellbore.

5.2. Linear solvers

In our simulator, a family of CPR-type preconditioners are implemented. Among all the CPR-type preconditioners, the CPR-FPF preconditioner is considered as the most efficient one (Wang et al., 2015; Liu et al., 2016). The application of CPR-FPF preconditioner to the linear systems resulted from black-oil model problems is stated in (Wang et al., 2015; Liu et al., 2016). For the compositional model, the natural variables (Coats et al, 1980) are employed as the primary unknowns in our simulator, then the matrix J can be represented as a similar form:

$$J = \begin{pmatrix} J_{wp} & J_{ws_w} & J_{wX_1} & 0 & \cdots & 0 \\ J_{c_1p} & J_{c_1s_w} & J_{c_1X_1} & J_{c_1,X_2} & \cdots & J_{c_1,X_{n-1}} \\ \cdots & \cdots & \cdots & \cdots & \cdots & \cdots \\ J_{c_np} & J_{c_ns_w} & J_{c_nX_1} & J_{c_n,X_2} & \cdots & J_{c_n,X_{n-1}} \end{pmatrix}, \tag{19}$$

where, n is the number of components, $X_i, i = 1,\ldots,n-1$ are the primary variables. If only oil phase exists, $X_i, i = 1,\ldots,n-1$ are the component mole fractions in oil phase $x_i, i = 1,\ldots,n-1$; If only gas phase exists, $X_i, i = 1,\ldots,n-1$ are the component mole fractions in gas phase $y_i, i = 1,\ldots,n-1$; If oil and gas phases coexist, X_1 is the gas phase saturation, and $X_i, i = 2,\ldots,n-1$ are the component mole fraction of gas phase $y_i, i = 1,\ldots,n-2$. The alternative block factorization (ABF) decoupling method (Bank et al., 1989) used as the preprocessing step to weaken the strong nonlinear coupling between the pressure unknowns and other unknowns in compositional model can be written as $D^{-1}Jx = D^{-1}b$, where

$$D = \begin{pmatrix} \mathbf{D}(J_{wp}) & \mathbf{D}(J_{ws_w}) & \mathbf{D}(J_{wX_1}) & 0 & \cdots & 0 \\ \mathbf{D}(J_{c_1p}) & \mathbf{D}(J_{c_1s_w}) & \mathbf{D}(J_{c_1X_1}) & \mathbf{D}(J_{c_1,X_2}) & \cdots & \mathbf{D}(J_{c_1,X_{n-1}}) \\ \cdots & \cdots & \cdots & \cdots & \cdots & \cdots \\ \mathbf{D}(J_{c_np}) & \mathbf{D}(J_{c_ns_w}) & \mathbf{D}(J_{c_nX_1}) & \mathbf{D}(J_{c_n,X_2}) & \cdots & \mathbf{D}(J_{c_n,X_{n-1}}) \end{pmatrix}, \tag{20}$$

and $\mathbf{D}(\cdot)$ stands for a diagonal matrix. Then, the algebraic multigrid (AMG) method is used to solve the submatrix corresponding to the pressure unknowns, and an ILU method is used to solve the full linear system both before and after the AMG method.

Besides the CPR-type preconditioners, the ILU preconditioner is also considered as an efficient method due to its low computational cost and has been used as the default preconditioner by some commercial simulators. In (Wang et al., 2015), the CPR preconditioner, the CPR-FPF preconditioner and the ILU preconditioner are compared. The numerical experiments in (Wang et al., 2015) show that (1) the CPR-FPF preconditioner is more efficient than the CPR preconditioner; (2) the ILU preconditioners may result in hundreds of linear iterations or even fail to achieve the required accuracy for large-scale reservoir simulations with highly heterogeneous permeability. However, when a CPR-type preconditioner is used, taking the CPR-FPF preconditioner as an example, the AMG and ILU methods need to be initialized before the linear iterations, and one AMG solution process and two ILU solution processes should be employed at each linear iteration. Compared with the ILU preconditioner, the CPR-FPF preconditioner has much larger computational cost. Hence, for the linear systems that are easy to solve, this drawback may results in more computational time for the CPR-FPF preconditioned linear solvers even it employs fewer linear

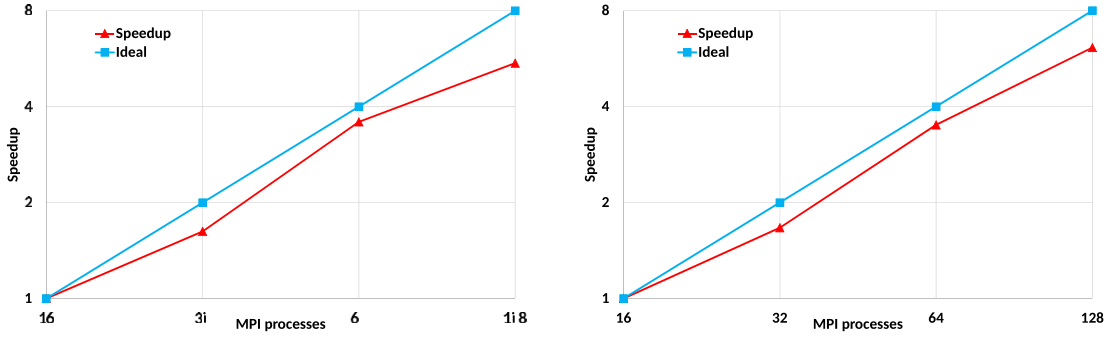

Fig. 11. Speedup of the refined SPE9 case.

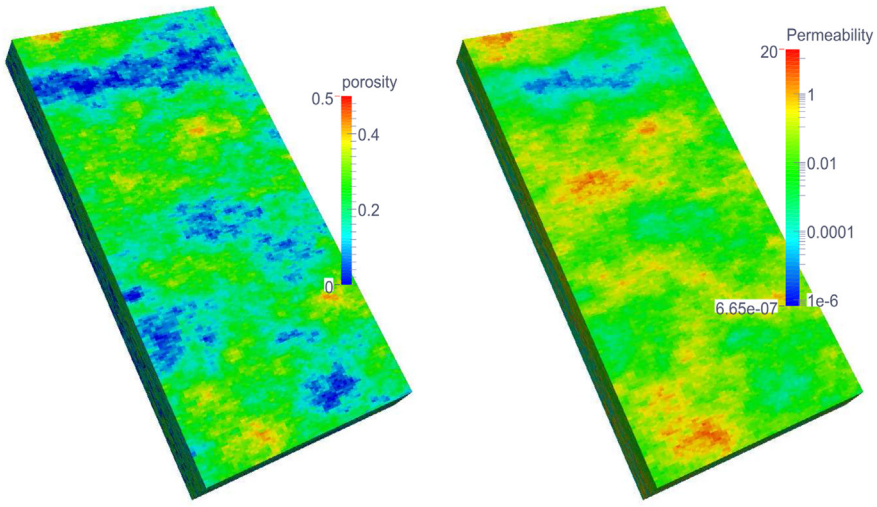

(a) porosity (b) permeability

Fig. 12. SPE10 geological information.

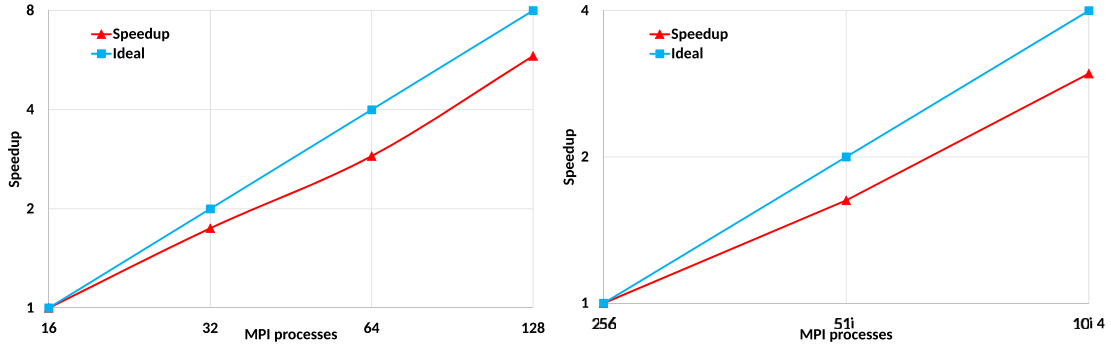

(a) SPE10 (b) SPE10-R2

Fig. 13. Speedup of the SPE10-based black oil model cases.

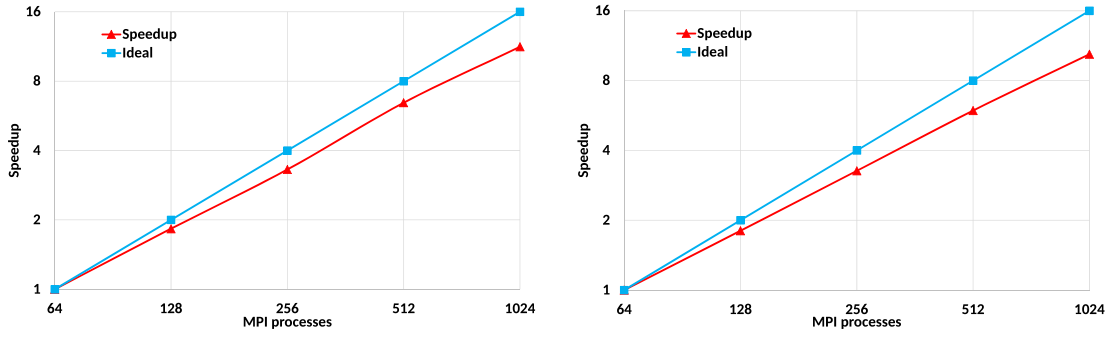

(a) CPR-FPF (b) Adaptive

Fig. 14. Speedup of the MX521X469 case.

iterations. Even for the difficult problems, since the inexact Newton method is employed by our simulator, the stop criteria of linear iterations depending on the residual of each nonlinear iteration may be relatively large, such as 10^{-1}, and the ILU preconditioned linear solver is capable of achieving the required accuracy efficiently. To overcome this drawback, an adaptive preconditioning strategy, which is capable of automatically selecting preconditioner between the CPR-type preconditioners and the ILU preconditioners, is developed to further improve the computational efficiency. The main idea of this adaptive strategy is to use an indicator $\varepsilon_{a,r}$ to decide the difficult level of solving a linear system. For a linear system resulted from a Newton iteration at each time step, the indicator $\varepsilon_{a,r}$ is defined as

$$\varepsilon_{a,r} = \frac{\varepsilon_a}{\varepsilon_a^0}, \tag{21}$$

where ε_a is the initial absolute residual of this linear system, and ε_a^0 is the initial absolute residual of the linear system resulted from the first Newton iteration of this time step. If $\varepsilon_{a,r}$ is larger than a switch criteria ε_s, which is set to be 10^{-3} in our computation, we assume the linear system is relatively easy to solve, and as a consequence the RAS-ILU preconditioner is used; otherwise, the CPR-type preconditioners should be used. A safeguard for the ILU preconditioners, which is call the expected iteration times $\mathcal{N}_e$, is also used in case of the failure of the ILU preconditioned linear solvers. An expected convergence rate R_e can be calculated by

$$R_e = \varepsilon^{\frac{1}{\mathcal{N}_e}}, \tag{22}$$

where ε is the stop criteria of the linear iterations. If the convergence rate e of the linear solver is larger than R_e, the ILU preconditioners will be switched to the CPR-type preconditioners. Full description of this adaptive preconditioner strategy is written in Algorithm 1. Restarted GMRES(m) method and the CPR-FPF preconditioner are used as representative linear solver and the CPR-type preconditioner in Algorithm 1, and any other linear solvers and CPR-type preconditioners can be used as alternate.

6. Parallel implementation

Our simulator is built on a parallel platform PRSI (Liu et al., 2015), which is written by C language and MPI (Message Passing Interface). PRSI is designed for large-scale reservoir simulations and provides grid management module, parallel input and output module, linear solver module, matrix/vector module and well management module. The structure of our simulator is shown in Fig. 3.

For parallel computation on distributed memory computers, the computational domain must be partitioned. The grid partitioning methods usually have two major goals. The first one is to create partitions with equal numbers of gird cells on each processor, which ensures that each processor has an equal computational load and communicates with other processors at the same time. The second one is minimize the number of neighbouring blocks on each partition, which can reduce the chances for network. These two aspects are both essential to the parallel scalability for large-scale problems. In (Wang et al, 2014a), a new approach to address dynamic load imbalance in parallel compositional simulation is developed for implicit-pressure/explicit-saturation (IMPES) scheme. Since fully implicit schemes are employed for both black oil models and compositional models, the linear solver would dominate the computation. Our main concern of the grid partitioning is to guarantee the partitioning quality and reduce the networking. One of the core techniques employed in the grid management module is the Hilbert Spacing-filling Curve (HSFC) method for grid partitioning. The HSFC method is a geometry information based method, which has good spatial locality, takes low computational cost and guarantees the partitioning quality, The HSFC method can be described the following three steps:

- Use a linear mapping to map the computational domain Ω to a cube $(0,1)^3$;
- Employ the Hilbert method to define a map from the cube $(0,1)^3$ to a line (0,1);
- Partition the line (0,1) into N_p (N_p is the number of processors) sub-intervals that has the same amount of cells.

More details about the HSFC method can be found in (Liu, 2008). Another popular open source software, METIS/ParMETIS (Karypis et al.,), is also supported by our simulator as an alternative grid partitioning method.

All the data related with the grid, such as the porosity and the permeability, are distributed into each MPI process, as well as the matrix and the vector resulted from the Jacobian. For the matrix, the dense storage and compressed sparse row storage (both sequential and parallel versions) are supported.

The simulation results are outputted in two types of files. The first type of files is for visualization. The physical variables, such as pressure and saturation, at each selected time step are outputted by the Visualization Toolkit (VTK) format. In order to keep the parallel efficiency of the entire simulation computation, the output process is totally parallelized. The VTK files can be read by some open source softwares, such as Paraview (Henderson et al., 2004). All the well data, such as oil production rate and bottom-hole pressure, and numerical performance, such as the number of linear iterations and time cost, are written in text files. These output files can provide valuable information for reservoir engineers to optimize the oil/gas production.

For the linear solvers, Krylov subspace methods, including the GMRES method and the BiCGSTAB method are implemented. The AMG method used in our simulator is the BoomerAMG from HYPRE (Yang, 2002; Falgout and Yang, 2002). The ILU methods, including ILU(k) and ILUT methods, are implemented and used in the CPR-FPF preconditioner. For sequential computation, the ILU methods can be applied directly. When the parallel computation is employed, due to the sequential nature of the ILU methods, the domain decomposition methods (Elli and Widlund, 2005) should be used and the ILU method is considered as a subdomain solver. The restricted additive Schwarz (RAS) method (Cai and Sarkis, 1999) is one of the most commonly used domain decomposition methods, and is implemented in our platform. We use RAS-ILU to represent the restricted additive Schwarz method with ILU method as the subdomain solver. Besides the general propose preconditioners, a family of CPR-type preconditioners, such as the CPR preconditioner, the CPR-FPF preconditioner (Wang et al., 2015) and the fast auxiliary space preconditioner (FASP) (Hu et al., 2011), are also implemented. The adaptive linear solver is the default linear solver in our simulator. For parallel computation, the ILU preconditioner R^{-1} will be replaced by the RAS-ILU preconditioner.

7. Numerical experiments

In this section, we first use six examples to validate the mathematical models and features supported by our simulator. The numerical experiments show good matches between the results of our simulator and that of a commercial simulator. To demonstrate the computational efficiency and parallel scalability of our simulator, large-scale problems are tested on parallel computers, encouraging parallel scalability and speedup are obtained. We also compare the CPR-type preconditioners and the adaptive preconditioning strategy. From the numerical performance, we can conclude that our adaptive preconditioning strategy can significantly improve the computational efficiency.

7.1. Validation of black-oil-based and compositional cases

Six examples are selected to validate our simulator. Example 1, 2, 3, and 4 are used to test the standard black oil model, api tracking model, gas condensate model and compositional model, respectively. Example 5 has three cases, which are used to test the dual-porosity model, dual-porosity dual-permeability model and the MINC model. Example 6 is employed to re-exam the standard black

oil model on a corner point grid. Example 2, 3 and 5 are from Computer Modeling Group (CMG) Ltd. The results of our simulator are compared with that of IMEX black oil simulator and GEM compositional simulator from CMG. In Figs. 4–10, we use "PRSI-BOS" (for black-oil models) and "PRSI-COMP" (for compositional models) to represent the results of our simulator.

Example 1. The first SPE comparative solution project (Odeh et al, 1981). This case has $10 \times 10 \times 3 = 300$ gird cells, constant porosity and layered permeability. There is one producer operating with maximum oil rate 20,000 STB/day and minimum bottom-hole pressure 1000 psia and one gas injector operating with maximum gas rate 100 MMSCF/day and maximum bottom-hole pressure 10,000 psia. The simulation time is 10 years.

Example 2. API tracking case, MXSMO019 from CMG. This case has $11 \times 1 \times 11 = 121$ gird cells, constant porosity and permeability. One producer is considered in this case. It operates with maximum oil rate 2000 STB/day and minimum bottom-hole pressure 1020 psia. The initial light component concentration is layered as (1.0, 0.77, 0.69, 0.61, 0.53, 0.47, 0.39, 0.31, 0.23, 0.15, 0.0). The simulation time is 10 years.

Example 3. Gas condensate case, MXSMO036 from CMG. This case has $3 \times 3 \times 1 = 9$ gird cells, constant porosity and permeability. One well is located at the center of the domain. The well performs as a producer at the first 3600 days operating with maximum gas rate 50 MMSCF/day and minimum bottom-hole pressure 350 psia, then turns into a gas injector operating with maximum gas rate 70.5 MMSCF/day and maximum bottom-hole pressure 4006.47 psia. The simulation time is 8000 days.

Example 4. The third SPE comparative solution project (Kenyon et al, 1987). This case has $9 \times 9 \times 4 = 324$ gird cells, constant porosity and layered permeability. Ten components are considered. Peng-Robinson EOS is used in this case. There is one producer opreating with maximum gas rate 6200 MSCF/day and minimum bottom-hole pressure 500 psia and one cycling gas injector opreating with maximum gas rate 4700 MSCF/day and maximum bottom-hole pressure 4000 psia. The simulation time is 4900 days.

Example 5. Dual-porosity/dual-permeability/MINC cases, MXFRR008/007/003 from CMG. The grid has $10 \times 10 \times 1 = 100$ gird cells. The fracture spacing is 100 ft in all the x, y and z directions. One producer operate with maximum liquid rate 300 STB/day and minimum bottom-hole pressure 15 psia. One water injector operates with maximum water rate 500 STB/day.

Example 6. The ninth SPE comparative solution project (Killough et al, 1995). Corner point grid is used in this case, which has $24 \times 25 \times 15 = 9000$ gird cells. 25 producers and one water injector are considered in this case: the maximum oil rate of all the producers is 1500 STB/day at the first 300 days, then lowered to 100 STB/day, and finally raised back to 1500 STB/day at the 900th day; the maximum water injection rate of the injector is 5000 STB/day. The simulation time is 900 days.

For the SPE1 case, Fig. 4 shows the oil production rate, GOR (gas/oil ratio) and bottom-hole pressure of the producer. The results exactly match. For the API tracking case, we compared the bottom-hole pressure of the producer, the oil production rate and the light component production rate, Fig. 5. The results well match. For the gas condensate case, Fig. 6 shows the pressure, dew point pressure and the oil phase saturation at the well block. During the production, the oil component condenses from the gas phase along with the reservoir pressure depletion. Since the well begins to inject gas, the reservoir pressure rises, and the oil component begins to vaporize into the gas phase. In Fig. 7, the oil production rate and the bottom-hole pressure match the results of IMEX. For the compositional model case, SPE3, the oil production rate and the bottom-hole pressure of the producer are compared with GEM, and the results well match; see Fig. 8. For the dual-porosity/dual-permeability/MINC cases, the oil production rate is compared with IMEX, and the results well match; see Fig. 9. For the SPE9 case, we randomly select four producers and compare their oil production rate with IMEX. The results match; see Fig. 10.

There are little differences that we may observe from the comparison between our results and CMG's. The reasons that cause the differences may be various, such as different PVT table and relative permeability table interpolations, different implicit schemes, and different convergence critera. Despite the existing of little differences, the agreement and matches of the results demonstrate the correctness of our simulator.

7.2. Solver and large-scale parallel efficiency tests

Numerical experiments in this section are tested on the cluster GPC (General Purpose Cluster) from Canada's largest supercomputer center SciNet (Loken et al., 2010). The GPC consists of 3780 nodes (IBM iDataPlex DX360M2) with a total of 30,240 cores (Intel Xeon E5540) at 2.53 GHz, with 16 GB RAM per node (some larger-memory nodes up to 32 GB). Our jobs were run on the nodes with 16 GB memory connected with non-blocking DDR InfiniBand. The 16 GB memory and 8 cores of each employed node are fully used in our computation, and each MPI process runs on a core.

In Tables 1–7, "NP" is the number of MPI processes employed in the computation, "Steps" is the total number of time steps, "Newton" is the number of Newton iterations, "Linear" is the number of linear solver iterations, "Avg. L." is the average number of linear solver iterations per Newton iteration, "Time" is the total computational time, and "Scal." is the parallel scalability.

7.2.1. Refined SPE9 case

In this case, each grid cell of the SPE9 case is refined into 64 gird cells, which results in 576,000 gird cells in total. The simulation time is 300 days. For this case, we use from 16 to 128 MPI processes. In Table 1, we tested the CPR-FPF preconditioner. Since this case only contains half a million gird cells, the linear systems are relatively easy to solve. The CPR-FPF preconditioned GMRES method only employs an average of 3 or 4 linear iterations for each linear system. The parallel scalability is excellent when up to 64 MPI processes are used. When 128 MPI processes are employed, each subdomain only contains less than 5000 gird cells, and the time of communication between MPI processes may be huge, which results in the drop of the parallel scalability. For this case, we also tested the adaptive preconditioning strategy, and the results are shown in Table 2. As we can see, the adaptive preconditioning strategy uses some ILU preconditioners to replace the CPR-type preconditioner. Although the number of linear iterations increases, the computational time is saved as we expect. The speedup of the refined SPE9 case can be seen in Fig. 11.

7.2.2. SPE10-based cases

The geological information of the tenth SPE comparative project (SPE10) is used to test the robustness of our nonlinear and linear solvers, as well as the parallel efficiency of large-scale problems. SPE10 is a challenging test case due to its highly heterogeneous permeability and porosity. Its permeability varies between 6.65×10^{-11} and 20 Darcy, and its porosity varies between 0 and 0.5, see Fig. 12. The dimensions are $1200 \times 2200 \times 170$ (ft) and it has 1.1 million ($60 \times 220 \times 85$) gird cells. The top 35 layers (70 ft) represent the Tarber formation and the bottom 50 layers (100 ft)

represent the Upper Ness formation. Four producers are placed at four corners of the reservoir, and one injector in the center. The total simulation time is 2000 days. More details can be found in (Christie et al, 2001). The original SPE10 case, a oil-water two-phase case, is modified to a black-oil three-phase case.

For this case, we use from 16 to 128 MPI processes, and the numerical results are shown in Table 3. The CPR-FPF preconditioner is used in this case. We can see that the number of nonlinear and linear iterations is almost the same during the increase of the MPI processes, which can demonstrate the robustness of our nonlinear and linear solvers. From 16 to 128 MPI processes, the computational time is almost halved when doubling the number of MPI processes, and more than 70% parallel scalability is achieved. In order to test a larger case, each grid cell of the SPE10-based black oil model case is refined into 9 gird cells, which results in a case containing $120 \times 440 \times 170 = 8{,}976{,}000$ gird cells. We represent this case as SPE10-R2. Considering the size of this case, from 256 to 1024 MPI processes are employed. The CPR-FPF preconditioner is also used in this refined case. Because of the limitation of the computational resource, 300 time steps are simulated. The robust performance of our nonlinear and linear solver, as well as encouraging parallel scalability are obtained again from the numerical results shown in Table 4. The speedup of these two SPE10-based black oil model cases are shown in Fig. 13.

With the SPE-R2 case, we test the adaptive strategy, and the results are shown in Table 5. We can see that the number of total linear iterations does not have significant increase, and even decreases when 1024 MPI processes are employed. However, half of the CPR-type preconditioners are replaced by the ILU preconditioners. Benefiting from the low computational cost of the ILU preconditioners, around 20% computational time is saved.

7.2.3. A black-oil large-scale case involving hundreds of wells

In the subsection, a water flooding case is considered. The first one, the MX521X469 case, contains $512 \times 469 \times 20 = 4.88$ million gird cells, as well as 90 water injection wells and 110 production wells. The porosity and permeability are both constant for this case. The simulation time is 2000 days. More details about this case can be found in (Brown et al., 2015). The efficiency and scalability of the design of our simulator for cases with hundreds of wells are tested by using from 64 to 1024 MPI processes.

In Table 6, the CPR-FPF preconditioner is used. We can see that the robustness of the nonlinear and linear solvers is not affected by the number of the wells. The parallel scalability is also good even when 1024 MPI processes are used. The adaptive strategy is also test in this case, Table 7. Due to the constant permeability of this case, the linear systems are much more easier to solve, which is captured by the adaptive strategy. The adaptive solver employs a large number of ILU preconditioners to replace the CPR-FPF preconditioners, and saves about 15% computational time. The speedup of the MX521X469 case can be seen in Fig. 14.

8. Conclusions

In this paper, a parallel multi-continuum black oil and compositional simulator is designed and implemented for large-scale parallel reservoir simulations. Both the Cartesian grid and the corner point grid are supported by our simulator. HSFC method is implemented for the parallel grid partition. The black-oil-based models and compositional model, as well as the fracture models and a geomechanics interface are involved in the simulator. An inexact Newton method is used to solve the strongly coupled nonlinear systems, which can avoid the linear system oversolved. A new preconditioning technique, which combines the CPR-type preconditioners and a new adaptive preconditioning strategy, is developed to improve the computational efficiency and save the computational time. The simulator is validated by comparing benchmarks with commercial simulators IMEX and GEM by CMG. The large-scale problems, the refined SPE9 case, SPE10-based black oil cases and a case with hundreds of wells, illustrate that our new linear system solution methods are more efficient and our simulator is scalable.

Acknowledgment

The support of Department of Chemical and Petroleum Engineering, University of Calgary and Reservoir Simulation Research Group is gratefully acknowledged. The research is partly supported by NSERC/AIEES/Foundation CMG, AITF iCore, IBM Thomas J. Watson Research Center, and the Frank and Sarah Meyer FCMG Collaboration Center for Visualization and Simulation. The research is also enabled in part by support provided by WestGrid (www.westgrid.ca), SciNet (www.scinethpc.ca) and Compute Canada Calcul Canada (www.computecanada.ca).

References

Bank, R.E., Chan, T.F., Coughran Jr., W.M., Smith, R.K., 1989. The alternate-block-factorization procedure for systems of partial differential equations. BIT Numer. Math. 29 (4), 938–954.
Behie, G.A., Forsyth Jr., P., 1984. Incomplete factorization methods for fully implicit simulation of enhanced oil recovery. SIAM J. Sci. Stat. Comput. 5 (3), 543–561.
Beraldo, V.T., Blunt, M.J., Schiozer, D.J., Qi, R., et al., 2007. Streamline simulation with an api tracking option. In: EUROPEC/EAGE Conference and Exhibition. Society of Petroleum Engineers.
Brown, G.L., Collins, D.A., Chen, Z., et al., 2015. Efficient preconditioning for algebraic multigrid and red-black ordering in adaptive-implicit black-oil simulations. In: SPE Reservoir Simulation Symposium. Society of Petroleum Engineers.
Cai, X.-C., Sarkis, M., 1999. A restricted additive schwarz preconditioner for general sparse linear systems. SIAM J. Sci. Comput. 21 (2), 792–797.
Cao, H., Tchelepi, H.A., Wallis, J.R., Yardumian, H.E., et al., 2005. Parallel scalable unstructured cpr-type linear solver for reservoir simulation. In: SPE Annual Technical Conference and Exhibition. Society of Petroleum Engineers.
Chen, Z., Huan, G., Ma, Y., 2006. Computational methods for multiphase flows in porous media. SIAM 2.
T. Chen, N. Gewecke, Z. Li, A. Rubiano, R. Shuttleworth, B. Yang, X. Zhong, Fast Computational methods for reservoir flow models.
Christie, M., Blunt, M., et al., 2001. Tenth spe comparative solution project: a comparison of upscaling techniques. In: SPE Reservoir Simulation Symposium. Society of Petroleum Engineers.
Coats, K.H., et al., 1980. An equation of state compositional model. Soc. Petrol. Eng. J. 20 (05), 363–376.
Cominelli, A., Casciano, C., Panfili, P., Rotondi, M., Bosco, P., et al., 2014. Deployment of high-resolution reservoir simulator: methodology & cases. In: Abu Dhabi International Petroleum Exhibition and Conference. Society of Petroleum Engineers.
Dean, R.H., Gai, X., Stone, C.M., Minkoff, S.E., et al., 2006. A comparison of techniques for coupling porous flow and geomechanics. SPE J. 11 (01), 132–140.
DeBaun, D., Byer, T., Childs, P., Chen, J., Saaf, F., Wells, M., Liu, J., Cao, H., Pianelo, L., Tilakraj, V., et al., 2005. An extensible architecture for next generation scalable parallel reservoir simulation. In: SPE Reservoir Simulation Symposium. Society of Petroleum Engineers.
Dogru, A.H., Sunaidi, H.A., Fung, L.S., Habiballah, W.A., Al-Zamel, N., Li, K.G., 2002. A parallel reservoir simulator for large-scale reservoir simulation. SPE Reserv. Eval. Eng. 5 (1), 11–23.
Dogru, A.H., Fung, L.S.K., Middya, U., Al-Shaalan, T., Pita, J.A., 2009. A next-generation parallel reservoir simulator for giant reservoirs. In: SPE/EAGE Reservoir Characterization & Simulation Conference.
Elli, A., Widlund, O.B., 2005. Domain Decomposition Methods: Algorithms and Theory, vol. 3. Springer, Berlin.
Falgout, R., Yang, U., 2002. hypre: a library of high performance preconditioners. Comput. Sci. 2002, 632–641.
Fussell, D., Yanosik, J.L., et al., 1978. An iterative sequence for phase-equilibria calculations incorporating the redlich-kwong equation of state. Soc. Petrol. Eng. J. 18 (03), 173–182.
Gilman, J.R., Kazemi, H., et al., 1983. Improvements in simulation of naturally fractured reservoirs. Soc. Petrol. Eng. J. 23 (04), 695–707.
Gutierrez, M., Lewis, R., Masters, I., et al., 2001. Petroleum reservoir simulation coupling fluid flow and geomechanics. SPE Reserv. Eval. Eng. 4 (03), 164–172.
Henderson, A., Ahrens, J., Law, C., et al., 2004. The ParaView Guide. Kitware Clifton Park, NY.
Hu, X., Liu, W., Qin, G., Xu, J., Zhang, Z., et al., 2011. Development of a fast auxiliary subspace pre-conditioner for numerical reservoir simulators. In: SPE Reservoir

Characterisation and Simulation Conference and Exhibition. Society of Petroleum Engineers.
Jiang, J., Shao, Y., Younis, R.M., et al., 2014. Development of a multi-continuum multi-component model for enhanced gas recovery and Co_2 storage in fractured shale gas reservoirs. In: SPE Improved Oil Recovery Symposium. Society of Petroleum Engineers.
J. Jiang, R. Younis, et al., Hybrid coupled discrete-fracture/matrix and multi-continuum models for unconventional-reservoir simulation, SPE J..
Kaarstad, T., Froyen, J., Bjorstad, P., Espedal, M., 1995. Massively parallel reservoir simulator. In: SPE Reservoir Simulation Symposiuma, San Antonio, Texas.
G. Karypis, K. Schloegel, V. Kumar, Parmetis: parallel graph partitioning and sparse matrix ordering library, Version 1.0, Dept. of Computer Science, University of Minnesota.
Kenyon, D., et al., 1987. Third spe comparative solution project: gas cycling of retrograde condensate reservoirs. J. Petrol. Technol. 39 (08), 981–997.
Killough, J.E., Bhogeswara, R., 1991. Simulation of compositional reservoir phenomena on a distributed-memory parallel computer. J. Petrol. Technol. 43 (11), 1368–1374.
Killough, J.E., Camilleri, D., Darlow, B.L., Foster, J.A., 1997. Parallel reservoir simulator based on local grid refinement. In: SPE Reservoir Simulation Symposium, Dallas.
Killough, J., et al., 1995. Ninth spe comparative solution project: a reexamination of black-oil simulation. In: SPE Reservoir Simulation Symposium. Society of Petroleum Engineers.
Li, K., Dogru, A., McDonald, A., Merchant, A., Al-Mulhem, A., Al-Ruwaili, S., Sobh, N., Al-Sunaidi, H., 1995. Improving the performance of mars simulator on cray-2 supercomputer. In: SPE Middel East Oil Show in Bahrain, 11–14 March.
Liu, H., 2008. Dynamic load balancing on adaptive unstructured meshes. In: 10th IEEE International Conference on High Performance Computing and Communications.
Liu, H., Wang, K., Chen, Z., Jordan, K.E., Luo, J., Deng, H., et al., 2015. A parallel framework for reservoir simulators on distributed-memory supercomputers. In: SPE/IATMI Asia Pacific Oil & Gas Conference and Exhibition. Society of Petroleum Engineers.
Liu, H., Wang, K., Chen, Z., 2016. A family of constrained pressure residual preconditioners for parallel reservoir simulations. Numer. Linear Algebra Appl. 23 (1), 120–146.
Loken, C., Gruner, D., Groer, L., Peltier, R., Bunn, N., Craig, M., Henriques, T., Dempsey, J., Yu, C.-H., Chen, J., et al., 2010. Scinet: Lessons Learned from Building a Power-efficient Top-20 System and Data Centre. In: Journal of Physics: Conference Series, 256. IOP Publishing, p. 012026.
Luo, J., Chen, Z., Wang, K., Deng, H., Liu, H., et al., 2015. An efficient and parallel scalable geomechanics simulator for reservoir simulation. In: SPE/IATMI Asia Pacific Oil & Gas Conference and Exhibition. Society of Petroleum Engineers.
Luo, J., Wang, K., Liu, H., Chen, Z., 2016. Coupled geomechanics and fluid flow modeling in naturally fractured reservoirs. In: Low Permeability Symposium. Society of Petroleum Engineers.
Mehra, R., Heidemann, R., Aziz, K., 1983. An accelerated successive substitution algorithm. Can. J. Chem. Eng. 61 (4), 590–596.
Michelsen, M.L., 1982. The isothermal flash problem. part I. stability. Fluid Phase Equilibria 9 (1), 1–19.
Minkoff, S.E., Stone, C.M., Bryant, S., Peszynska, M., Wheeler, M.F., 2003. Coupled fluid flow and geomechanical deformation modeling. J. Petrol. Sci. Eng. 38 (1), 37–56.
Moinfar, A., Varavei, A., Sepehrnoori, K., Johns, R.T., et al., 2013. Development of a coupled dual continuum and discrete fracture model for the simulation of unconventional reservoirs. In: SPE Reservoir Simulation Symposium. Society of Petroleum Engineers.
Odeh, A.S., et al., 1981. Comparison of solutions to a three-dimensional black-oil reservoir simulation problem (includes associated paper 9741). J. Petrol. Technol. 33 (01), 13–25.
Parashar, M., Wheeler, J.A., Pope, G., Wang, K., Wang, P., 1997. A new generation eos compositional reservoir simulator: Part ii framework and multiprocessing. In: Paper SPE 37977 Presented at the SPE Reservoir Simulation Symposium, Dallas, June 8–11.
Peaceman, D.W., et al., 1983. Interpretation of well-block pressures in numerical reservoir simulation with nonsquare grid blocks and anisotropic permeability. Soc. Petrol. Eng. J. 23 (03), 531–543.
Peng, D.-Y., Robinson, D.B., 1976. A new two-constant equation of state. Ind. Eng. Chem. Fundam. 15 (1), 59–64.
Pruess, K., et al., 1985. A practical method for modeling fluid and heat flow in fractured porous media. Soc. Petrol. Eng. J. 25 (01), 14–26.
Redlich, O., Kwong, J.N., 1949. On the thermodynamics of solutions. v. an equation of state. fugacities of gaseous solutions. Chem. Rev. 44 (1), 233–244.
Rutledge, J.M., Jones, D.R., Chen, W.H., Chung, E.Y., 1991. The use of massively parallel simd computer for reservoir simulation. In: SPE Paper 21213 Presented at the Eleventh SPE Symposium on Reservoir Simulation, Anaheim.
Saad, Y., 1981. Krylov subspace methods for solving large unsymmetric linear systems. Math. Comput. 37 (155), 105–126.
Shiralkar, G., Stephenson, R., Joubert, W., Lubeck, O., van Bloemen Waanders, B., 1997. A production quality distributed memory reservoir simulator. In: SPE Reservoir Simulation Symposium.
Soave, G., 1972. Equilibrium constants from a modified redlich-kwong equation of state. Chem. Eng. Sci. 27 (6), 1197–1203.
Stüben, K., 2001. A review of algebraic multigrid. J. Comput. Appl. Math. 128 (1), 281–309.
Stueben, K., Clees, T., Klie, H., Lu, B., Wheeler, M.F., et al., 2007. Algebraic multigrid methods (amg) for the efficient solution of fully implicit formulations in reservoir simulation. In: SPE Reservoir Simulation Symposium. Society of Petroleum Engineers.
Tran, D., Nghiem, L., Buchanan, L., et al., 2009. Aspects of coupling between petroleum reservoir flow and geomechanics. In: 43rd US Rock Mechanics Symposium & 4th US-Canada Rock Mechanics Symposium. American Rock Mechanics Association.
Wallis, J., Kendall, R., Little, T., et al., 1985. Constrained residual acceleration of conjugate residual methods. In: SPE Reservoir Simulation Symposium. Society of Petroleum Engineers.
Wallis, J., et al., 1983. Incomplete gaussian elimination as a preconditioning for generalized conjugate gradient acceleration. In: SPE Reservoir Simulation Symposium. Society of Petroleum Engineers.
Wang, K., Liu, H., Chen, Z., 2015. A scalable parallel black oil simulator on distributed memory parallel computers. J. Comput. Phys. 301, 19–34.
Wang, Y., Killough, J.E., et al., 2014a. A new approach to load balance for parallel/compositional simulation based on reservoir-model overdecomposition. SPE J. 19 (02), 304–315.
Wang, C., Wu, Y.-S., et al., 2014b. Modeling analysis of transient pressure and flow behavior at horizontal wells with multi-stage hydraulic fractures in shale gas reservoirs. In: SPE Unconventional Resources Conference. Society of Petroleum Engineers.
Warren, J., Root, P.J., et al., 1963. The behavior of naturally fractured reservoirs. Soc. Petrol. Eng. J. 3 (03), 245–255.
Wheeler, J.A., Smith, R.A., October, 1989. Reservoir simulation on a hypercube. In: SPE 19804 Presented at the 64th Annual SPE Conference & Exhibition, SanAntonio.
Winterfeld, P., Wu, Y., 2014. Simulation of CO_2 sequestration in brine aquifers with geomechanical coupling. In: Computational Models for CO_2 Sequestration and Compressed Air Energy Storage, pp. 275–303.
Wu, Y.-S., Qin, G., Ewing, R.E., Efendiev, Y., Kang, Z., Ren, Y., et al., 2006. A multiple-continuum approach for modeling multiphase flow in naturally fractured vuggy petroleum reservoirs. In: International Oil & Gas Conference and Exhibition in China. Society of Petroleum Engineers.
Wu, Y.-S., Di, Y., Kang, Z., Fakcharoenphol, P., 2011. A multiple-continuum model for simulating single-phase and multiphase flow in naturally fractured vuggy reservoirs. J. Petrol. Sci. Eng. 78 (1), 13–22.
Wu, Y.-S., Li, N., Wang, C., Ran, Q., Li, J., Yuan, J., et al., 2013. A multiple-continuum model for simulation of gas production from shale gas reservoirs. In: SPE Reservoir Characterization and Simulation Conference and Exhibition. Society of Petroleum Engineers.
Wu, Y.-S., Li, J., Ding, D., Wang, C., Di, Y., et al., 2014. A generalized framework model for the simulation of gas production in unconventional gas reservoirs. SPE J. 19 (05), 845–857.
Wu, Y.-S., Pruess, K., et al., 1988. A multiple-porosity method for simulation of naturally fractured petroleum reservoirs. SPE Reserv. Eng. 3 (01), 327–336.
Xiong, Y., Fakcharoenphol, P., Winterfeld, P., Zhang, R., Wu, Y.-S., et al., 2013. Coupled geomechanical and reactive geochemical model for fluid and heat flow: application for enhanced geothermal reservoir. In: SPE Reservoir Characterization and Simulation Conference and Exhibition. Society of Petroleum Engineers.
Xiong, Y., Winterfeld, P., Wang, C., Wu, Y.-S., Huang, Z.-Q., 2015. A compositional model fully coupled with geomechanics for liquid-rich shale and tight oil reservoir simulation. In: SPE Reservoir Simulation Symposium. Society of Petroleum Engineers.
Yang, U.M., 2002. Boomeramg: a parallel algebraic multigrid solver and preconditioner. Appl. Numer. Math. 41 (1), 155–177.